Validation of PET-Acquired Input Functions for Cardiac Studies

I.N. Weinberg*, S.C. Huang, E.J. Hoffman, L. Araujo†, C. Nienaber, M. Grover-McKay‡, M. Dahlbom, and H. Schelbert

UCLA School of Medicine, Los Angeles, California

To validate the determination of the arterial input function by noninvasive dynamic PET imaging, measurements of blood-pool activity in canine LV by PET were compared to beta probe measurements of arterial blood withdrawn directly from the LV. PET scans were done during intravenous bolus injections of [^{13}N]ammonia or ^{82}Rb, while the activity of blood withdrawn continuously from a catheter inserted in the LV was measured with a beta probe. PET determinations of LV blood-pool activity were compared with dispersion-corrected beta probe time-activity curves. In 15 experiments involving four dogs under a wide range of physiologic conditions, LV time-activity curves obtained with PET matched well in shape with those obtained with the beta probe. Linear regression yielded slopes within 10% of unity (95% confidence interval) and high correlation ($r > 0.968$, $p < 0.001$). We conclude that noninvasive measurement of the arterial input function by dynamic PET imaging is valid.

J Nucl Med 29:241–247, 1988

The determination of regional myocardial blood flow with noninvasive positron emission tomography (PET) measurements utilizing bolus injections requires the time-activity curve of the tracer in arterial blood (*1,2*). The arterial input function can be determined from a sequence of withdrawn arterial blood samples by counting in a well counter. Other methods yielding an arterial input function of high temporal resolution include continuously monitored withdrawn arterial blood (for brain imaging) (*3–5*), and region of interest (ROI) calculation from dynamically—acquired PET images of the left ventricular (LV) chamber in cardiac studies (*2*).

The aim of this study was the validation of the noninvasive measurement of arterial time-activity curves obtained with dynamic PET cardiac imaging, by comparison with activity curves obtained independently with a beta probe that measured radioactivity in blood continuously withdrawn from the LV. The low sensitivity of the beta probe to background radiation allowed measurement of blood activity in the immediate vicinity of the probe without contamination from gamma rays originating in the body of the experimental animal. The dispersion due to the beta probe tubing was removed mathematically from the raw data by deconvolution to get the arterial input function.

Received Apr. 30, 1987; revision accepted Aug. 20, 1987.

For reprints contact: Heinrich R. Schelbert, MD, Div. of Nuclear Medicine, UCLA School of Medicine, Los Angeles, CA 90024.

* Present address: University of Miami, Miami, FL.

† Present address: Hammersmith Hospital, London, England.

‡ Present address: Long Beach VA Hospital, Long Beach, CA.

MATERIALS AND METHODS

Beta Probe

The positron-sensitive probe shown in Figure 1 was built to measure the concentration of activity in blood (*6*). The probe consisted of a plastic scintillator (BC-412 scintillator material, Bicron Corp., Newbury, OH) machined to cylindrical shape 2 cm in diameter and 3 cm in length. The scintillator was coupled with optical glue (Epo-Tek 302 adhesive, Epoxy Technology Inc., Billerica, MA) to a photomultiplier (R1166 Photomultiplier, Hammamatsu Corp.) and covered with light-tight, thin-walled, shrink-fit tubing. The scintillator and photomultiplier were seated in a cylindrical high-density alloy (Ostalloy-158, Semi-Tech, Inc., Garland, TX) casing with 3 cm minimum wall thickness. Sterile polyethylene tubing (INTRAMEDIC tubing, Clay Adams Div. of Becton Dickinson Co., Parsippany, NJ) (1.14 mm ID, 1.57 mm OD) was tightly looped around the scintillator. The beta probe housing design allowed the tubing to be looped three to seven times around the detector while maintaining sterility. A lower number of loops gave less dispersion at a cost of reduced detection efficiency. The experiments described below were conducted with three or four loops. The length of tubing between the dog heart and beta probe was minimized (total length 30 to 90 cm) to reduce dispersion. Blood was withdrawn through the tubing at constant flow (5 ml/min for [^{13}N] ammonia, and

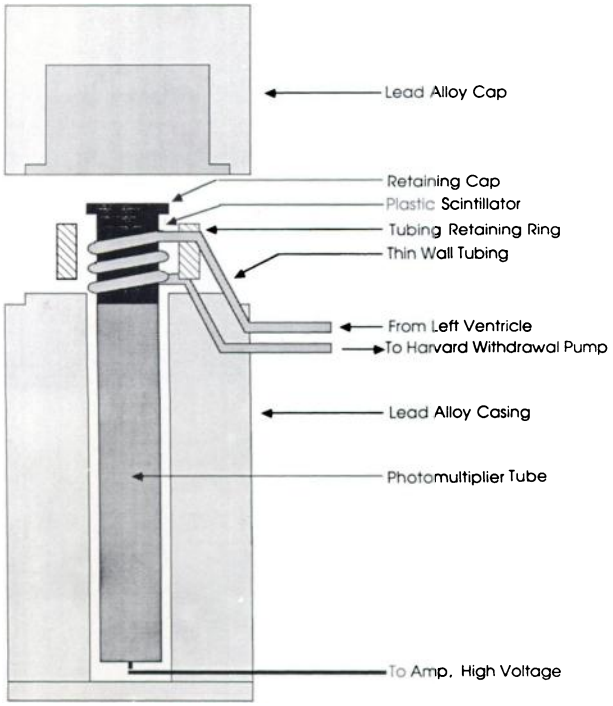

FIGURE 1
Side view of beta probe. Thin-walled polyethylene tubing carrying blood from dog LV is looped around plastic scintillator. Scintillator and attached photomultiplier are shielded by high density housing.

3.9 ml/min for rubidium-82 experiments) with a Harvard pump (Harvard Apparatus, Millis, MA).

With an energy threshold greater than 350 keV, the response of the plastic scintillator (7) to positrons was between 10 and 100 times greater than its response to 511 keV gamma radiation. Thus, use of the plastic scintillator allowed selective detection of positrons from the thin-walled tubing adjacent to the detector while minimizing the contribution of 511 keV gamma radiation from the experimental animal. A factor of ten reduction in sensitivity to 511 keV gamma background was provided by high-density alloy shielding surrounding the beta probe. The signal from the photomultiplier was amplified and measured with a single channel analyzer, whose output was fed to a scaler module. The scaler was read and cleared every collection cycle (cycle time: 1–4 sec) by a DEC MicroVaxII computer. The threshold for the single channel analyzer was set between 500 and 700 keV. The detectors were calibrated with known spectral peaks of iodine-131, cesium-137, cobalt-57, technetium-99, and gallium-68, and showed good linearity between photomultiplier output and gamma ray energy (correlation coefficient 0.987, $p < 0.001$). The maximum scaler count rate for the experiments described below was 15,000/sec. The accuracy of the data collection system was experimentally verified for count rates as high as 100,000/sec.

Animal Preparation

Four mongrel dogs, weighing 20 to 30 kg, were anesthetized with sodium pentobarbitol (25 mg/kg), intubated and ventilated with room air. Fine polyethylene tubing (1.14 mm ID, 1.57 mm OD) was advanced through a puncture wound into the left ventricle and used for continuous withdrawal of arterial blood. To reduce clotting in the beta probe tubing, either the dog was heparinized prior to the study, or the lines were flushed with heparinized saline before and after each study. A total of 15 dynamic studies were done, consisting of four nitrogen-13 (^{13}N) ammonia (radioactive half-life 9.96 min) studies each on two dogs, three rubidium-82 (^{82}Rb) (radioactive half-life 75 sec) studies on one dog, and four ^{82}Rb studies on another dog. Scans were performed while resting and under conditions of high and low blood flow obtained by the administration of dipyridamole (0.56 mg/kg intravenously over 4 min) and morphine (0.5 to 1.5 mg/kg intravenously).

Study Procedure

For correction of photon attenuation, transmission scans were made with the ECAT III PET scanner (Computed Tomography Inc., Knoxville, TN) after positioning the dog. For the [^{13}N]ammonia experiments, 5 mCi of [^{13}N]ammonia were injected intravenously over 15 sec, followed by a saline flush. For the ^{82}Rb experiments, ~10 mCi of ^{82}Rb from a $^{82}Sr/^{82}Rb$ generator (Squibb Sr/Rb Infusion System, Squibb Diagnostics, New Brunswick, NJ) were injected intravenously as a bolus. The dynamic PET acquisition, the withdrawal of arterial blood, and the initial intravenous injection of tracer, were initiated simultaneously. The withdrawal of arterial blood was maintained for 5 min. The dynamic PET scan protocol for the [^{13}N]ammonia experiments consisted of 15 6-sec acquisitions, five 18-sec acquisitions, and six 60-sec acquisitions. The dynamic PET scan protocol for the ^{82}Rb experiments consisted of 14 4-sec acquisitions, six 15-sec acquisitions, and six 30-sec acquisitions. The rates of coincident, random, and multiple events detected by the tomograph were recorded for later use in correcting for dead-time losses. To reduce noise caused by the limited number of counts per dynamic study frame, a reconstruction filter was applied (Hanning filter, 50% to 60% Nyquist frequency cutoff) which yielded a nominal image resolution of 15 mm (FWHM).

Beta Probe Dispersion Measurement

At the end of the animal study, the dispersion of the tracer through the withdrawal apparatus was measured. Dog blood was withdrawn through the withdrawal apparatus from a vial. Enough blood was withdrawn to fill the tubing, and then the infusion pump was shut off to allow the blood to come to rest. A small volume of [^{13}N]ammonia or ^{82}Rb (corresponding in type to the radioisotope used for the study) was added to the blood in the vial and the vial was shaken vigorously. The withdrawal of blood from the vial was then resumed, to provide a step function of radioactivity in blood. The time-activity curve measured by the probe gave the dispersion and delay due to the tubing.

Calibration of the Beta Probe Efficiency Against the Tomography Efficiency

After the dispersion measurement, the tubing was flushed with saline. A small volume of the radioisotope used in the study was added to a water-filled cylinder. Fluid from the cylinder was withdrawn through the withdrawal apparatus, and the activity measured by the beta probe. Simultaneously, the cylinder was placed in the field of view of the tomograph, and scanned with PET. The relative values between the PET and beta probe measurements yielded a calibration constant K^{eff} between the PET scanner and the beta probe.

DATA ANALYSIS AND RESULTS

Determination of Input Function

The time-activity curves measured by the beta probe is the convolution of the true arterial input function and the dispersion due to the withdrawal apparatus. Deconvolution was employed to obtain the true arterial input function. To allow straightforward deconvolution, all data were decay-corrected for physical decay of the radioisotope. Splined analytic functions were fitted (least-squares regression) to the time-activity curves. To reduce the deleterious effects of noise the deconvolution (described below) was applied to the analytic functions, rather than to the original time-activity curves (*8*). After deconvolving for dispersion, the physical decay was reintroduced to the data to facilitate direct comparison with the tomographic measurements. The physical decay of the radioisotope is thus not explicitly indicated in the following summary of the deconvolution technique.

Summary of the Deconvolution Technique

Let m(t) be a combination of analytical functions which fits the decay-corrected measured step function response of the beta probe. The impulse response function g(t) of the beta probe apparatus is then the derivative of m(t). Let f(t) be the true arterial input function, and h(t) the measured blood curve. Then h(t) is the convolution (*) of f(t) and g(t):

$$h(t) = \int_0^t f(\tau)\, g(t - \tau)\, d\tau \equiv f(t)*g(t).$$

Taking the Fourier transform, and letting F(k), G(k), and H(k) be the Fourier transforms of f(t), g(t), and h(t), respectively, one obtains H(k) as the product of F(k) and G(k), allowing one to solve for F(k):

$$F(k) = H(k)/G(k).$$

The inverse Fourier transform of F(k) is f(t).

Calculation of the Impulse Function from the Measured Step Response Function

To remove the influence of noise on the deconvolution processing, the measured step function was corrected for the physical decay of the radioisotope and then fit to the following function:

$$m(t) = \begin{cases} 0 & t \le t_{delay} \\ k_{magnitude} \cdot (1 - \exp(-k_{step} \cdot (t - t_{delay}))) & t > t_{delay} \end{cases}.$$

The delay time t_{delay} was defined to be the time that the beta probe count rate in the step function measurement exceeded some set fraction (between 1% and 25%, depending on the noise environment and the beta probe collection duration) of the peak count rate. A least-squared nonlinear regression program was used to adjust the parameters $k_{magnitude}$ and k_{step} to minimize the difference between the above function and the measured curve. A typical measured and fitted step function for [^{13}N]ammonia (corrected for physical decay of the radioisotope) is shown along with the corresponding impulse function g(t) in Figure 2. The impulse function was calculated with the following function, with the parameters k_{step} and t_{delay} determined as described above:

$$g(t) = \begin{cases} 0 & t \le t_{delay} \\ (1/k_{step}) \cdot \exp(-k_{step} \cdot (t - t_{delay})) & t > t_{delay} \end{cases}.$$

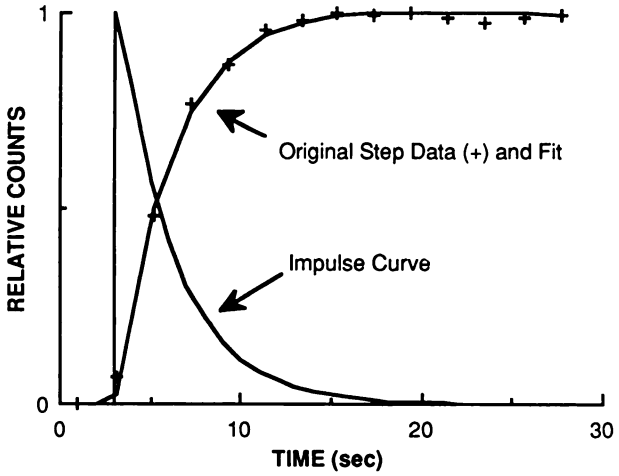

FIGURE 2
The first processing step applied to the beta probe data for a typical [^{13}N]ammonia study is illustrated. A curve fit to a decay-corrected measured step function (+) was differentiated to yield a decay-corrected impulse function.

Fit of the Measured Beta Probe Blood Curve

The treatment of the decay-corrected measured beta probe blood curve was similar to that applied to the decay-corrected step function response. After removal of leading zeroes corresponding to the initial delay, a composite function with eight (for [^{13}N]ammonia) or seven (for ^{82}Rb) adjustable parameters was used to fit the data. The rising section of the data was fit with a Compertz function (*9*), and the falling section of the data fit with a double exponential. For [^{13}N]ammonia experiments an adjustable parameter was added to the falling section to represent a constant term. The composite function was evaluated over a set of time points (with Δt = 1 sec) to give a blood curve. A typical [^{13}N]ammonia blood curve measured by the beta probe as well as the corresponding fitted curve is shown in Figure 3A.

Fourier Manipulation of the Beta Probe Data

Before Fourier transformation, the fitted curve was extended to 512 sec (two to four times the original collection period) according to the functional form of the fitted analytic functions. This was done to increase the sampling resolution of the frequency representation of the curves in order to reduce the incidence of artifacts (*10*). After inverse Fourier transformation of the ratio H(k)/G(k) to yield f(t), negative numbers in f(t) were set to zero. As a check on the procedure, the resulting arterial function (Fig. 3A) was convolved (in the time domain) with the impulse function, and the result of this convolution compared to the measured arterial blood curve, as shown in Figure 3B. The resulting calculated true arterial function was integrated over the time intervals corresponding to the tomograph data collection time intervals, to facilitate direct comparison with the tomograph-acquired blood-pool data.

Processing of the Tomograph Blood Pool Data

Regions of interest (ROIs) for the myocardium were drawn on PET images acquired late in the scan when the blood activity is lower than the myocardial activity (Image D of Fig. 4). LV blood-pool regions clearly separate from the myocar-

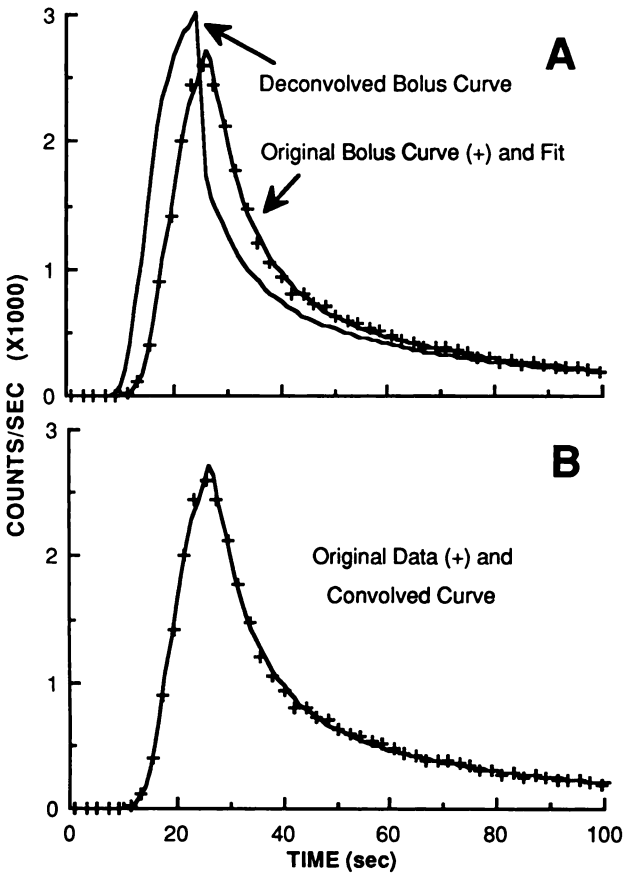

FIGURE 3
Additional processing steps applied to the [^{13}N]ammonia study beta probe data are illustrated in this figure. A: Observed beta probe data from a bolus [^{13}N]ammonia injection (+) were fitted to yield a smooth bolus curve. The fitted bolus curve was decay corrected and deconvolved with the decay-corrected impulse curve (see Fig. 2) to obtain a decay-corrected deconvolved bolus curve. To facilitate comparison with the original bolus curve, the deconvolved bolus curve is shown in this figure with decay reintroduced. B: As a test on the deconvolution routine, the decay-corrected deconvolved bolus curve was convolved with the decay-corrected impulse curve. The resulting decay-corrected convolved curve is shown (smooth curve) with decay reintroduced to facilitate comparison with the original bolus curve (+).

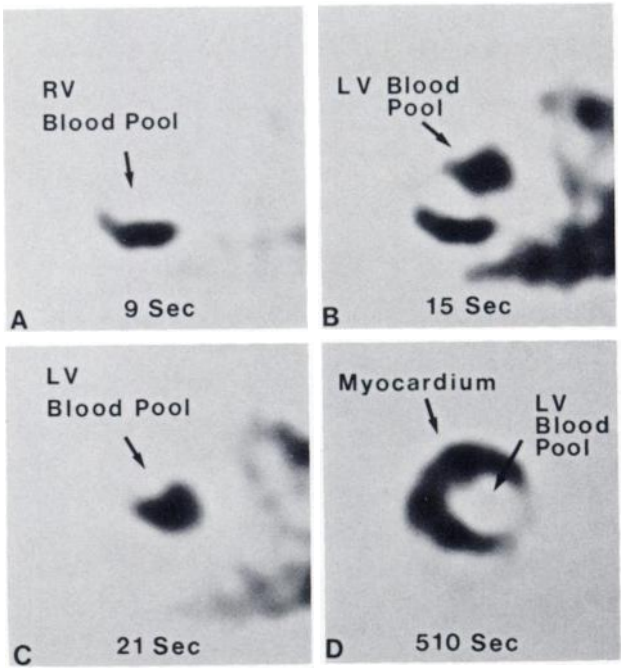

FIGURE 4
PET images acquired with [^{13}N]ammonia at various times after bolus injection. Early images (9, 15, and 21 sec into the scan) are displayed (A, B, and C) along with a late image (D, 510 sec into the scan). The image whose blood-pool value was maximal (B) was used to define the blood-pool region.

dial regions were then drawn around the sites of maximum activity in the early images when blood activity peaked and myocardial activity was low (Image B of Fig. 4). Blood-pool regions were drawn as small as possible to minimize spillover of counts from the myocardial regions in the image. The counts in each region of interest were divided by the scan acquisition time interval. The counts were further corrected for scanner deadtime (*11*).

Comparison Between Beta Probe and PET Data

The PET ROI blood-pool data were multiplied by K_{eff} (beta probe efficiency/tomograph efficiency) and compared to the beta probe blood-pool data. Figures 5A and 5B show the good agreement in shape, timing of the initial bolus, and magnitude, between the PET and beta probe data for typical [^{13}N]ammonia and ^{82}Rb studies.

The data from all the time points (n = 136) of the eight [^{13}N]ammonia studies, and from all the time points (n = 126) of the seven ^{82}Rb studies were plotted in scatter plots, as shown in Figures 6A and 6B, for [^{13}N]ammonia and ^{82}Rb studies, respectively. In [^{13}N]ammonia experiments on two dogs, with a total of eight bolus injections (17 time points/experiment), results yielded a correlation coefficient of 0.968 ($p < 0.001$), and a slope of 1.032 ± 0.046 (95% slope confidence interval). In ^{82}Rb experiments on two dogs, with a total of seven bolus injections under a wide range of physiologic conditions (18 time points/experiment), time-activity curves obtained with PET and deconvolved beta probe measurements matched well in shape, with a correlation coefficient of 0.975 ($p < 0.001$), and a slope of 1.092 ± 0.044 (95% slope confidence interval).

As a result of the large slope of the arterial blood curves near the peaks, small errors in timing resulted in large apparent deviations in the scatter plots. The good agreement of the data as obtained with the PET and beta probe measurements is probably underestimated with this statistical technique. An additional figure of merit is the fit between the time-integrated data obtained with PET and with the beta probe. The integral values were displayed in scatter plots between the results of PET and beta probe measurements, as shown in Figures 7A and 7B, for [^{13}N]ammonia and ^{82}Rb studies, respectively. For the [^{13}N]ammonia studies, the integrated arterial input functions had a correlation coefficient of 0.986 ($p < 0.001$), and a slope of 1.083 ± 0.185 (95% slope confidence interval). For

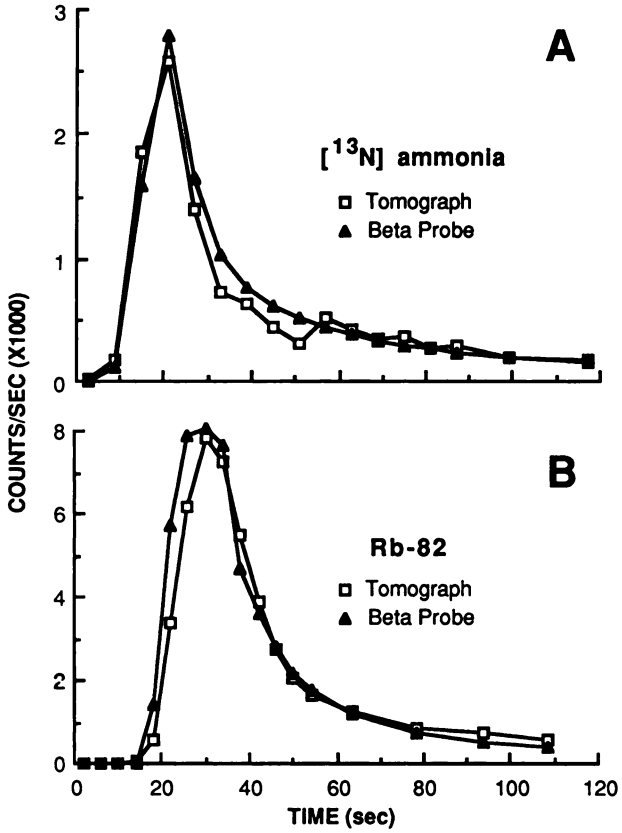

FIGURE 5
Comparison of typical [^{13}N]ammonia (A) and ^{82}Rb (B) arterial activity data obtained with the beta probe and with PET. A deconvolved beta probe curve which has had decay reintroduced (see Fig. 3A) was summed along intervals corresponding to the tomographic acquisition intervals to yield an arterial time-activity curve (triangles). This curve is shown along with deadtime corrected tomograph data (squares).

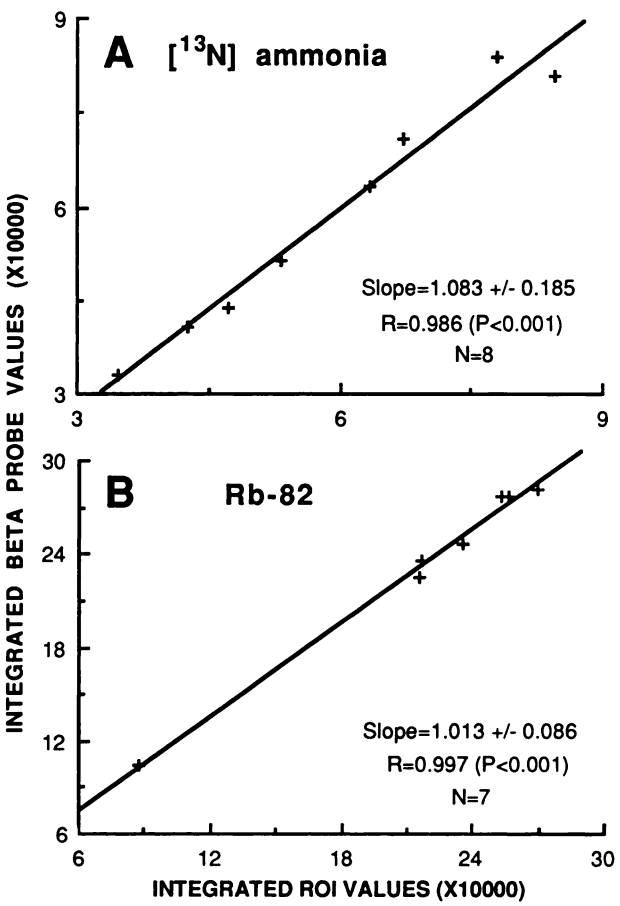

FIGURE 6
Comparison between the beta probe and PET determinations of arterial activity data at all time points for all the [^{13}N]ammonia (A) and ^{82}Rb (B) studies. Scatter plots are shown along with linear regressions. The slope confidence interval for the regression lines was 95%.

the ^{82}Rb studies, the integrated arterial input functions had a correlation coefficient of 0.997 ($p < 0.001$), and a slope of 1.013 ± 0.086 (95% slope confidence interval).

DISCUSSION

The determination of regional myocardial blood flow with noninvasive PET measurements utilizing bolus injections of activity requires knowledge of the shape, time dependence, and integral of the arterial input function. As this study indicates, measurements of arterial activity obtained with noninvasive PET cardiac imaging show high correlations with independent beta probe high-temporal resolution measurements of arterial blood activity obtained directly from the left ventricular blood pool. The results of this study not only pertain to measurements of bolus tracer administrations but also to other methods of tracer administration as for example a step function infusion.

Inspection of time-activity curves obtained with the two methods as in Figure 5 shows underestimation in PET data as compared to the beta probe data immediately after arrival of the bolus and overestimation of the activity at times late in the study. These phenomena are believed to be due to the partial volume effect (*12*), which at early times averages high blood-pool activity and low myocardial activity to effectively reduce apparent blood-pool activity, and which at late times averages low blood-pool activity and high myocardial activity to add activity to the blood-pool images. Supporting this thesis is the observation that underestimation of activity by PET at early times worsened when the ROI size of the blood pool was increased. In the present study, the blood-pool ROIs were drawn as small as possible to reduce errors from partial volume effect and heart wall motion. Also, when a plane was selected in which the LV blood pool ROI was close to the myocardium, the late PET measurements yielded larger overestimation than when planes were chosen in which the blood-pool ROI and the myocardium were farther apart. This is again consistent with the existence of spillover from

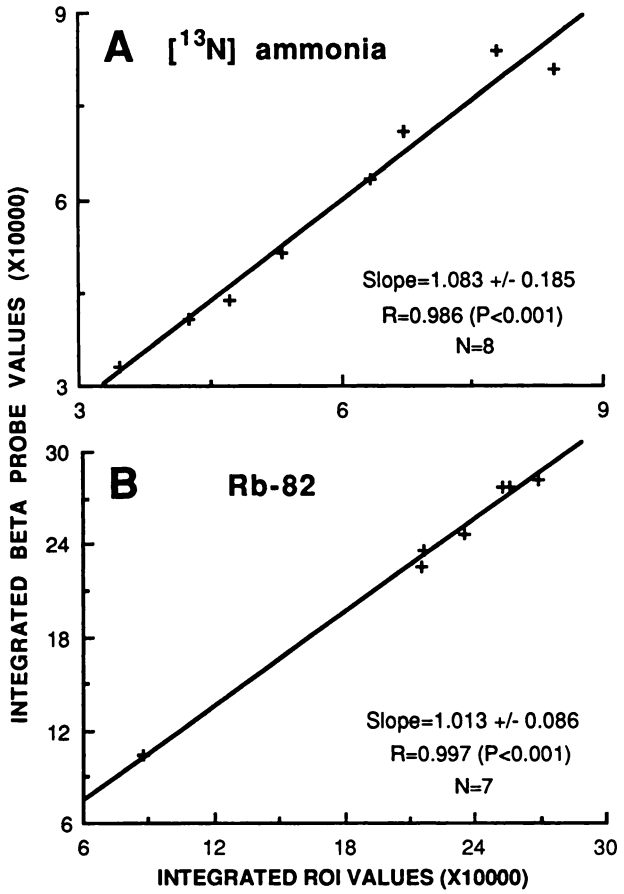

FIGURE 7
Comparison between time-integrated beta probe and PET determinations of arterial activity data for all the [^{13}N] ammonia (A) and ^{82}Rb (B) studies. Scatter plots are shown along with linear regressions. The slope confidence interval for the regression lines was 95%.

myocardium that causes discrepancy between the two measurements.

The partial volume effect and radioactivity spillover can be reduced in the present study by using a reconstruction filter of higher cutoff frequency in the image reconstruction. However, the image noise level will be increased and will result in noisier curves from the blood-pool ROI. In other words, there is a tradeoff between the noise level and the partial volume and spillover problem. In addition, it should be noted that similar tradeoffs occur for the tissue radioactivities in myocardium. Therefore, depending on the image noise level and the size of the blood pool, the selection of the image reconstruction filter and the ROI size should be carefully considered for quantitative measurement of the arterial input function. However, these problems for human cardiac studies are expected to be less, because of the larger LV blood-pool volume in humans.

Obviously, relatively low amounts of tracer activities were administered in the open chest dog experiments of the present study. Nevertheless, these amounts resulted in myocardial tracer uptake images of adequate quality. For studies in humans, administration of 10 to 15 mCi [^{13}N]ammonia yields comparable peak count rates. The image noise levels are also comparable between the present study and the human studies. For ^{82}Rb studies in humans, 30 to 50 mCi are usually required for adequate myocardial images and result in higher peak count rates. However, correction for dead-time losses at these high count rates is possible as described by Germano et al. (*11*).

In summary, independent measurements of activity of two radiotracers commonly used in PET cardiac imaging obtained directly from the left ventricular blood pool with high temporal resolution using a beta probe have validated the use of arterial input functions obtained noninvasively with cardiac PET imaging.

ACKNOWLEDGMENTS

The following assistance is acknowledged: R. Sumida, T. Ricci, K. Meadors, and G. Low (beta probe design), L. Bidaut and W. Digby (computations), F. Aguilar, L. Pang and C. Whitt (scans). This work was supported by Department of Energy Contract DE-AC03-76-SF00012 and NIH Grants HL-29845 and CA-42362. PET data were obtained in the Ahmanson Laboratory of Biochemical Imaging.

REFERENCES

1. Mullani NA, Goldstein RA, Gould KL, et al. Myocardial perfusion with Rb-82. I. Measurement of extraction fraction and flow with external detectors. *J Nucl Med* 1984; 24:901.
2. Phelps ME, Mazziotta JC, Schelbert HR, eds. Positron emission tomography and autoradiography. New York: Raven Press, 1986.
3. Kanno I, Lammertsma AA, Heather JD, et al. New York: Measurement of cerebral blood flow using bolus inhalation of $C^{15}O_2$ and positron emission tomography: description of the method and its comparison with the $C^{15}O_2$ continuous inhalation method. *J Cereb Blood Flow Metab* 1984; 4:224–234.
4. Hutchins GD, Hichwa RD, Koeppe RA. A continuous flow input function detector for $H_2{}^{15}O$ blood flow studies in positron emission tomography. *IEEE Trans Nucl Sci* 1986; 33:546.
5. Senda M, Nishizawa S, Yonekura Y, et al. Measurement of arterial time activity curves by monitoring continuously drawn arterial blood: errors and corrections. *J Nucl Med* 1986; 27:1001.
6. Lammertsma AA, Hoffman JM, Frakowiak RSJ, et al. A new dynamic technique to measure regional cerebral blood flow. *Thirteenth International Symposium on Cerebral Blood Flow and Metabolism*, June 1987.
7. Hurlbut CR. Plastic scintillators, a survey. American Nuclear Society, Winter Meeting, November 1985.
8. Raichle ME, Larson KB, Phelps ME, et al. In vivo measurement of brain glucose transport and metabolism employing glucose-C-11. *Am J Physiol* 1975; 228:1938–1945.
9. Draper N, Smith H. Applied regression analysis, 2nd

Ed. New York: John Wiley and Sons, 1981:511.
10. Bracewell RN. The fourier transform and its applications. New York: McGraw-Hill, 1978.
11. Germano G, Hoffman EJ. An investigation of count rate capability and dead time for a high resolution PET system. *J Nucl Med* 1987; 28:607.
12. Henze E, Huang SC, Ratib O, et al. Measurements of regional tissue and blood-pool radiotracer concentrations from serial tomographic images of the heart. *J Nucl Med* 1983; 24:987–996.